ELSEVIER

Catalysis Today 63 (2000) 71–85

CATALYSIS TODAY

www.elsevier.com/locate/cattod

Methane reforming with CO_2 over Ni/ZrO_2–CeO_2 catalysts prepared by sol–gel

J.A. Montoya [a,*], E. Romero-Pascual [b,1], C. Gimon [c], P. Del Angel [a], A. Monzón [b,2]

[a] *Instituto Mexicano del Petróleo, Simulación Molecular, Eje Central 152, Cp. 07730 Mexico D.F., Mexico*
[b] *Dpto. de Ingenieria Química y T.M.A., Facultad de Ciencias, Universidad de Zaragoza, 50009 Zaragoza, Spain*
[c] *L.P.M.C. URA-CNRS 474, Av. de l'Universite, 64000 Pau, France*

Received 1 November 1999; accepted 15 June 2000

Abstract

Ni/ZrO_2 catalysts promoted with different amounts of CeO_2 (0, 1, 8 and 20 wt.%) were prepared by the sol–gel method. The catalysts were characterized after calcination at 800°C and after reaction of CH_4 reforming with CO_2. Rietveld analysis reveals that the tetragonal ZrO_2 phase (t-ZrO_2) present in the catalysts is stabilized by the CeO_2, forming a solid solution, and avoiding transformation to the monoclinic phase (m-ZrO_2). Ni^{2+} also competes with Ce^{4+} in the incorporation to t-ZrO_2. The t-ZrO_2 stability increases with CeO_2 concentration. The catalyst activity is increased with the CeO_2 content, although some degree of deactivation, due mainly to the sintering of the support, was not completely avoided by ceria addition. The deposition of graphitic carbon does not play an important role in the catalysts deactivation. The catalytic performance is related to the Ni surface dispersion and NiO reducibility, both promoted by CeO_2 incorporation. CeO_2 enhances the reverse water-gas shift reaction during dry reforming of methane over the studied catalysts.

Keywords: Ni/ZrO_2–CeO_2 catalyst; Sol-gel; Dry reforming of methane; Reverse water-gas shift reaction

1. Introduction

In recent years, the CO_2 reforming of methane (dry reforming) has become an interesting alternative for the production of synthesis gas (H_2 and CO). This reaction produces a $H_2/CO \approx 1$, which is more suitable for obtaining sulfur-free synthetic liquid fuels (by the Fischer–Tropsch reaction) and valuable oxygenated chemicals than the H_2/CO ratio coming from the traditional steam reforming process [1]. Due to its endothermic nature, the major drawback of this reaction is the high temperature are required to reach high conversions. These drastic operating conditions provoke the deactivation of the catalyst by coke formation and/or sintering of the metallic phase and support [2,3]. In addition, it has been accepted that the catalytic activity depends on the nature of the support, active phase precursor, synthesis method, and pretreatment [3–5].

Nickel based catalysts have shown an excellent behavior in this reaction, with an activity comparable to noble metal catalysts [2,6]. Ni has been supported on different materials such as MgO, Al_2O_3, promoted-Al_2O_3, TiO_2, CeO_2, etc. However, most of these tend to deactivate by coke formation [2,3], which is closely related to the catalyst structure and

* Corresponding author.
E-mail addresses: amontoya@www.imp.mx (J.A. Montoya), amonzon@posta.unizar.es (A. Monzón).
[1] Tel.: +34-976-761157; fax: +34-976-762142.
[2] Same as Footnote 1.

0920-5861/00/$ – see front matter
PII: S0920-5861(00)00447-8

composition [7]. The use of supports with low concentration of Lewis acid sites and/or presence of basic sites, such as ZrO_2, MgO, and La_2O_3, resulted in enhanced activities, lower carbon deposition rates, and therefore more stable catalysts [8–10]. On the other hand, Swaan et al. [11] reported that activity of different Ni-based catalysts appears to depend essentially on the degree of reduction and the dispersion of Ni particles, and not so much on the support. More recently some studies [9,12–17] have pointed out that carbon formation is strongly diminished in catalysts with small as possible Ni particles. Another important fact in the catalyst life is the thermal stability of the support. In this respect, ZrO_2 has a high thermal stability as a catalyst support and its tetragonal phase, (t-ZrO_2), has both acid and basic properties [18]. In addition, it has been found that the t-ZrO_2 is the most active phase for some reactions [19], therefore is important to reduce at maximum the transition to the monoclinic phase, avoiding also the possible sintering of the support.

However, the t-ZrO_2 is considered to be a metastable phase and the transformation to monoclinic phase is complete at around 650–700°C. This change causes a drastic decrease of the surface area. The tetragonal or cubic phases can be stabilized by adding yttria, calcia, or ceria, thus maintaining small crystallite sizes due to their lower surface tension, and avoiding the transition to monoclinic form [20–22]. Calcia and ceria have basic surface properties and can act as catalytic promoters in Ni/Al_2O_3 catalysts [23,24].

In the present study we report the research about the activity, selectivity and carbon formation of Ni (15 wt.%)/ZrO_2 catalysts prepared by sol–gel and promoted with different amounts (0, 1, 8 and 20 wt.%) of CeO_2, during the reaction of methane reforming with CO_2. The catalysts have been characterized after calcination and after reaction in order to explain the effect of the CeO_2 addition on the catalysts activity.

2. Experimental section

2.1. Catalyst preparation

The catalysts were prepared by the sol–gel method. The precursors were $Ni(NO_3)_2{\cdot}6H_2O$, $Ce(NO_3){\cdot}6H_2O$, $Zr(OBu)_4$ (80 wt.%), HNO_3, supplied by Aldrich. The amount of each reactive was calculated in order to obtain 10 g of catalyst. The Ni content was 15 wt.% for all the catalysts, and the CeO_2 concentration was 0, 1, 8 and 20 wt.%. The preparation procedure was the following: a proper amount of $Zr(OBu)_4$ was dissolved in 700 ml of isopropyl alcohol (to keep a 2 wt.% ZrO_2 solution) and stirred for 2 h. The hydrolysis of the alkoxide solution was carried out at 5°C, adding dropwise a solution of H_2O ($H_2O/Zr(OBu)_4 = 4$ molar ratio), $Ni(NO_3)_2{\cdot}6H_2O$, $Ce(NO_3){\cdot}6H_2O$, HNO_3 ($HNO_3/Zr(OBu)_4 = 0.2$ molar ratio) and 100 ml of isopropyl alcohol. The green rigid transparent gels obtained were aged "in situ" for 24 h and then dried in air flow at room temperature. The dry gels were carefully calcined in air at 500°C during 2 h with a 100 Nml/min flow. In addition a Ni/CeO_2 catalyst was prepared by coprecipitation of a solution of Ni and Ce nitrates in isopropyl alcohol at constant pH = 9. The calcined solids were crushed and sieved and the fraction with particle size between 0.16 and 0.40 mm was kept. Finally, the samples were heated at 10°C/min and calcined in air at 800°C during 6 h with 50 ml air/min.

2.2. Characterization techniques

The specific surface area of the catalysts was measured by N_2 adsorption at 77 K with a Micromeritics Pulse Chemisorb 2700. The reducibility of NiO present in the catalysts calcined at 800°C was studied by temperature programmed reduction. The sample (200 mg) was heated at a rate of 5°C/min in a TPR system equipped with a TCD, from room temperature to 900°C, under a H_2 (6%)/N_2 mixture with a flow of 100 Nml/min. A NiO sample was examined by TPR for purposes of comparison with the catalysts. This sample was prepared from $Ni(NO_3)_2{\cdot}6H_2O$ by calcination under a N_2/H_2 mixture flow, as in the calcination of catalysts, from room temperature to 700°C at a rate of 10°C/min. The powder X-ray diffraction (XRD) patterns were recorded by Rigaku/Max Cu rotatory anode equipment. The Cu K$\alpha_{1,2} = 1.5418$ Å was obtained using a graphite secondary beam monochromator. In order to obtain the cell parameters and phase composition by using the Rietveld method, the diffractograms were measured under special

conditions. The scanning was made from $2\theta = 20$ to 110° with a 2θ step size of 0.02 and step time of 4 s. The samples were carefully placed on the sample holder to prevent inappropriate orientation. X-ray photoelectron spectroscopy (XPS) studies were carried out at room temperature with a SSI spectrometer (model 301), using Al Kα radiation. The spectrometer was equipped with a high temperature reaction cell to allow pretreatments. The samples were analyzed in the calcined and reduced state. To reduce the calcined catalysts the same reduction procedure was followed as that used in the catalytic experiments, as described in later. The samples were then transferred to the analysis chamber under an inert atmosphere. The analysis was done after the residual pressure of about 4×10^{-10} Torr was reached. The adventitious C 1s line at a binding energy of 284.6 eV was used as an internal standard. The TEM studies were carried out using a Jeol 100X equipment.

2.3. Catalytic evaluation

The catalysts behavior in CH_4 reforming with CO_2 was carried out in a conventional fixed-bed micro reactor system at atmospheric pressure. The reactor was a quartz tube with an internal diameter of 9 mm and the catalyst was supported on a quartz wool bed. The catalytic activity was measured at temperatures between 500 and 800°C. Also, stability experiments were carried out at 800°C, temperature at which (at thermodynamic equilibrium under the conditions described) carbon deposition is clearly diminished and stable nickel carbide formation is avoided [25]. Before the catalytic evaluation, the catalyst (100 mg in all cases) was reduced in situ at 500°C during 3 h with a mixture of $H_2 : N_2 = 50 : 50$ Nml/min. After this, for the catalytic evaluation at 500–800°C, the H_2 flow was turned off and purged with N_2 during 1 h. In the case of stability evaluations, the temperature was increased to 800°C with a heating rate of 10°C/min. The feed ratio was $CH_4 : CO_2 : N_2 = 1 : 1 : 4$ or $CH_4 : CO_2 : N_2 = 2 : 1 : 6$ with a total flow of 320 Nml/min and a space velocity (WHSV) of 190 800 lt/kg/h. A GC (HP 5890 series II) was used to analyze the reaction gas effluent at 20 min intervals. The GC used a thermal conductivity detector, with Argon as the carrier gas. A Carboxen 1000 column was used to separate the gas mixture.

The carbon formation on the catalysts during CH_4 reforming with CO_2 was studied in a thermogravimetric system operated as a differential reactor (CI Electronics Ltd., model MK2). All the experimental parameters, such as feed ratio ($CH_4 : CO_2 : N_2 = 1 : 1 : 4$), total flow, catalyst mass and reduction procedure were similar to those used in the micro reactor catalytic evaluation, with the exception of the reaction temperature, which was 700°C.

3. Results

3.1. Chemical analysis

The chemical composition of the catalysts was carried out by the plasma emission technique and the results are shown in Table 1. The NiO content of the catalysts ranged between 12.4 and 15 wt.%, except for the Ni/CeO_2 catalyst, where the NiO concentration was 18.3 wt.%.

3.2. Phase analysis by the Rietveld method

Fig. 1 shows the XRD patterns of the catalysts after calcination at 800°C. In the Rietveld analysis of diffraction data (Table 2) an anisotropic crystallite size effect was considered for all phases. It is observed that as the CeO_2 content increased, the t-ZrO_2 concentration was higher, whereas the content of monoclinic phase (m-ZrO_2) decreased. That means the presence of ceria in the Ni/ZrO_2 catalyst prevents or reduces the tetragonal-to-monoclinic transformation, and this fact becomes more evident as the CeO_2 content is higher (in the studied range). Thus, only the pure t-ZrO_2 was obtained in the Ni/ZrO_2–CeO_2-20 sample. In addition this catalyst presents some (1.4 wt.%) CeO_2 segregated. The NiO amount measured ranged from 10

Table 1
Chemical composition of the catalysts

Catalyst	ZrO_2	CeO_2	NiO
Ni/ZrO_2	87.6	–	12.4
Ni/ZrO_2–CeO_2-1	83.9	0.8	15.3
Ni/ZrO_2–CeO_2-8	78.3	7.8	13.9
Ni/ZrO_2–CeO_2-20	65.0	22.0	13.0
Ni/CeO_2	–	81.7	18.3

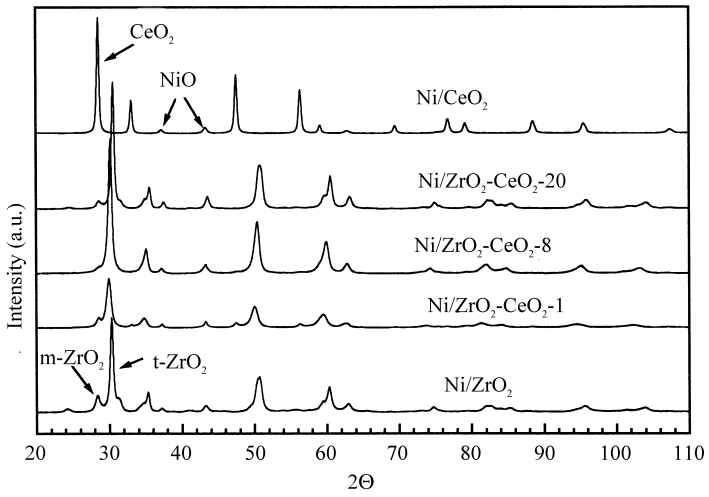

Fig. 1. XRD patterns of the catalysts calcined at 800°C.

Table 2
Results of Rietveld analysis. Phase composition (wt.%) of catalysts calcined at 800°C

Catalyst	t-ZrO_2 (%)	m-ZrO_2 (%)	CeO_2 (%)	NiO (%)
Ni/ZrO_2	66.17	22.5	–	11.14
Ni/ZrO_2–CeO_2-1	71.62	12.95	–	15.44
Ni/ZrO_2–CeO_2-8	84.54	5.10	–	10.36
Ni/ZrO_2–CeO_2-20	86.17	–	1.25	12.58
Ni/CeO_2	–	–	77.39	22.61

to 22 wt.%, which is similar to the nominal composition (Table 1). Thus most of the NiO crystallites are big enough to be detected by XRD.

The results of phase composition of the catalysts after reaction are shown in Table 3. As in the case of calcined catalysts, the higher amount of m-ZrO_2 was obtained in the samples with the lowest content of CeO_2 (Ni/ZrO_2 and Ni/ZrO_2–CeO_2-1). In these samples the m-ZrO_2 content was twice that of the calcined catalysts. This indicates that during the reaction the t-ZrO_2 crystallites grew and transformed into m-ZrO_2, in accordance with the Garvie's model [20]. However, the catalysts with 8 and 20 wt.% of CeO_2 did not show this trend, and the presence of m-ZrO_2 phase was not observed. In addition, in the Ni/ZrO_2–CeO_2-20 some CeO_2 remained segregated, though a part was incorporated into the t-ZrO_2 structure.

Table 3
Results of Rietveld analysis. Phase composition (wt.%) of catalysts after calcination and reaction at 800°C

Catalyst	t-ZrO_2	m-ZrO_2	CeO_2	Ni^0
Ni/ZrO_2	56.19	41.17	–	2.64
Ni/ZrO_2–CeO_2-1	67.33	29.06	–	3.61
Ni/ZrO_2–CeO_2-8	96.94	–	–	3.06
Ni/ZrO_2–CeO_2-20	96.91	–	0.5	2.59
Ni/CeO_2	–	–	94.55	5.45

As can be seen in Table 3, the quantities of Ni^0 measured in all the samples were lower than expected. The content of metallic nickel should be around 12 wt.%, according to the 15 wt.% average content of NiO obtained in the calcined catalysts (Table 2). This low value could be explained by the formation of small Ni^0 crystallites (smaller than 3 nm, and therefore not detectable by XRD) during the NiO reduction [26]. Also nickel is probably only reduced at surface and proximity, the bulk Ni remaining inaccessible to the gas. Another possibility is the incorporation of part of Ni into the structure of t-ZrO_2.

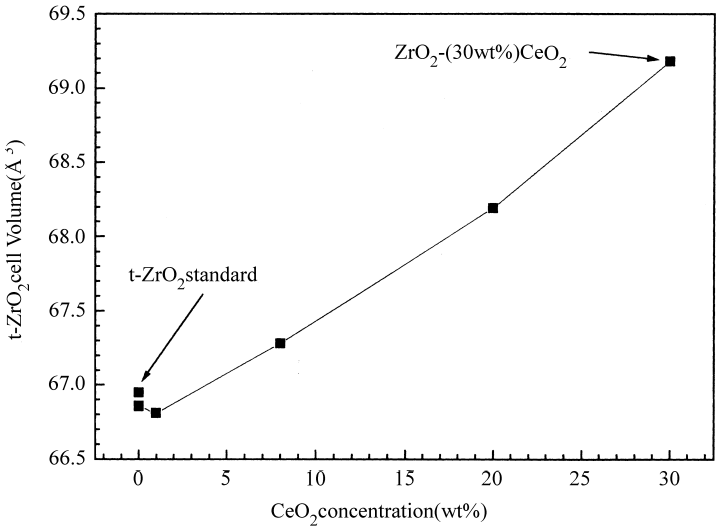

Fig. 2. Modification of t-ZrO_2 cell volume by the cation (Ce^{4+}, Ni^{2+}) incorporation in catalysts calcined at 800°C, calculated by Rietveld refinement of XRD data.

The cell parameters and cell volume (Fig. 2) of the t-ZrO_2 phase present in all the catalysts calcined at 800°C increased with the CeO_2 content, indicating that the CeO_2 was incorporated into the t-ZrO_2, forming a solid solution. In general, Vegard's law is widely accepted to confirm the presence of a solid solution. However, due to the variability of the c_0/a_0 ratio in the tetragonal system, the Vegard relationship is better applied to the cell volume rather than a single cell parameter (as used for the cubic system). Given that the ionic radii of Ce^{4+} (0.97 nm) is higher than that of the Zr^{4+} (0.84 nm), the cell volume of t-ZrO_2 should increase with the including of CeO_2, and this is what happened to the samples (Fig. 2). This confirms the Ce incorporation into the t-ZrO_2 lattice forming a solid solution. In addition, the t-ZrO_2 cell volume in Ni/ZrO_2 was smaller than that of the standard (pure) t-ZrO_2 (Fig. 2), pointing out that a fraction of Ni is also incorporated, given that the Ni^{2+} ionic radii (0.69 nm) is smaller than Zr^{4+}. It seems plausible that the t-ZrO_2 stabilization is carried out by Ce^{4+} incorporation into the host lattice and on the surface vacancies, which causes the surface free energy to decrease, thus avoiding the t-ZrO_2 crystallite growth. The presence of Ni^{2+} in the catalysts competes with Ce^{4+} for incorporation into the t-ZrO_2. Thus it is possible that a fraction of Ni^{2+} is included into the t-ZrO_2. The slight reduction observed in the Ni/ZrO_2–CeO_2-1 sample could be due to the incorporation of a small quantity of Ce^{+4} allowing the incorporation of a greater quantity of Ni^{+2}.

A sample of ZrO_2–(30 wt.%)CeO_2 (without Ni) was prepared using the same synthesis method and as expected it formed a complete solid solution. Its cell volume was higher than that of the Ni/ZrO_2–CeO_2-20 catalyst and did not follow the linear pattern of the Ni catalysts (see Fig. 2), confirming that part of the Ni^{2+} is incorporated into the t-ZrO_2 in all the catalysts. This fact also explains that part of the CeO_2 is segregated in the Ni/ZrO_2–CeO_2-20 catalyst. It has been found [27,28] that in the CeO_2–ZrO_2 system the solid solution formation and stability depend on the synthesis method. Thus, sol–gel was reported as the best method for preparing a $Zr_{0.25}Ce_{0.75}O_2$ stable phase [27].

3.3. Crystallite size evolution

Fig. 3 shows the evolution of the t-ZrO_2 crystallite size, present in all the samples, after the calcination process (800°C) and after reaction. The crystallite size was measured by Rietveld refinement considering the crystallite effect as isotropic. The horizontal line represents the critical crystallite size (22 nm) of the t-ZrO_2, below which the t-ZrO_2 is considered more stable, due to its lower surface energy, than the monoclinic

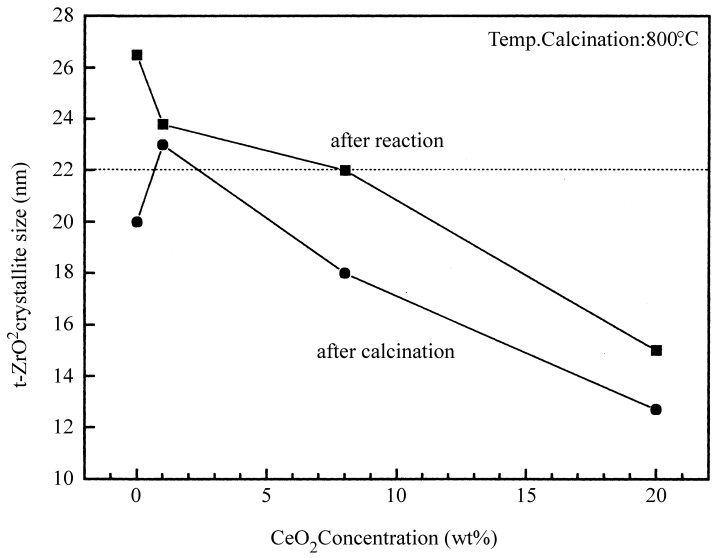

Fig. 3. Crystallite size evolution of t-ZrO_2 present in the Ni/ZrO_2–CeO_2 catalysts, as a function of temperature treatment and CeO_2 concentration.

phase [20]. Under a given treatment, the t-ZrO_2 crystallite size diminishes with the CeO_2 concentration. In the case of the Ni/ZrO_2 catalyst, the increase of the t-ZrO_2 crystallite size is the largest, suffering a strong process of sintering and transformation to the m-ZrO_2 phase. The lowest average crystallite size observed after each treatment is that of the Ni/ZrO_2–CeO_2-20 sample, which indicates that it has the highest thermal stability. The samples with a greater content of ceria undergo a similar increase in crystallite size (about 20%) despite having, before the reaction, crystallite sizes smaller than sample Ni/ZrO_2. On the other hand, this sample suffers a greater degree of sintering of the support in spite of the fact that its growth potential is much lower because the crystallite size is already large before reaction.

It is noteworthy that the Ni/CeO_2 catalyst exhibited the highest crystal size after calcination (about 35 nm) and that it continued growing during the reaction (after which the crystallite size reached a value of 48 nm). This result implies that this catalyst is not thermally stable.

Regarding the NiO crystallite size after calcination at 800°C, the mean size was similar for Ni/ZrO_2–CeO_2-1, Ni/ZrO_2–CeO_2-20 and Ni/CeO_2 catalysts (around 20.0 nm), but for the Ni/ZrO_2 and Ni/ZrO_2–CeO_2-8 catalysts, the value was smaller (around 15.0 nm). This indicates that the NiO is fairly well dispersed in all the catalysts and that the mean NiO crystallite size was not significantly affected by the support composition. However, the NiO crystallite size distribution is not necessarily the same. It is interesting to note that after reduction and reaction, the Ni^0 mean crystallite size (calculated from XRD) in all the samples was similar to the NiO mean size in calcined samples. According to the broadness of the Ni^0 reflection peaks it seems that an important fraction of Ni^0 had a low crystallite size, below the average size, and even below the XRD detection limit (3 nm). This partially explains the low Ni^0 concentration quantified from the XRD results and suggests that during the reduction stage and during the reaction, the sintering of the Ni^0 crystallites is not the dominant process, otherwise the shape of the reflection peaks would be different.

3.4. Surface area

The BET surface area results after calcination at 800°C showed some differences among the catalysts. Both Ni/ZrO_2 and Ni/ZrO_2–CeO_2-1 presented a 2 m^2/g surface area, while Ni/ZrO_2–CeO_2-8 and

Ni/ZrO_2–CeO_2-20 exhibited 6 and 5 m^2/g, respectively. Sample Ni/CeO_2 showed 1 m^2/g, in accordance to its lower thermal stability. As a general trend, it is observed ceria induces a slightly increase in the BET surface area of the samples. Rossignol et al. [27] have found that for CeO_2–ZrO_2 mixed oxides the surface area was independent of the synthesis method (coprecipitation and sol–gel) and the CeO_2 concentration. However for these materials the surface areas were considerably higher than the sol–gel NiO–ZrO_2–CeO_2 catalysts presented in this work, indicating that probably nickel can act as a nucleating agent promoting the sintering.

3.5. Surface composition and reducibility

Fig. 4 presents the results of temperature programmed reduction (TPR) of the catalysts calcined at 800°C. In this figure, for comparison, the TPR of the pure NiO sample is included, showing a definite peak at 360°C. For the Ni/CeO_2 catalyst a sharp peak at $T_{max} = 420$°C and other low-broad peak at $T_{max} = 800$°C were obtained. The first peak is associated with the reduction of NiO to Ni^0, and the peak at 800°C is related to the partial reduction of Ce^{+4} to Ce^{+3} [29,30]. The sharp peak obtained at 420°C corresponds to high uniformity in NiO crystallite size. This temperature is higher than that the reported by Tang et al. [31] for the same type of catalyst, which indicates a higher interaction between NiO and CeO_2 in our case. The rest of the samples showed a broader main reduction peak at higher temperature than that for the Ni/CeO_2. The wideness of the peak suggests a broad particle size distribution and, given that the reduction temperature is relatively high [26], can be concluded that it is associated to a more dispersed NiO exhibiting a stronger interaction with the support than the NiO present in the Ni/CeO_2 sample. This peak was slightly shifted to a higher T_{max} as the CeO_2 content increased. For the Ni/ZrO_2–CeO_2 catalysts an additional peak at lower temperature appeared. This is associated to larger NiO particles having a lower interaction with the support (reduction temperature closer to the pure NiO sample). For the Ni/ZrO_2–CeO_2-8 catalyst this peak at low temperature is shifted to a higher value, indicating that, for this sample, the Ni-support interaction was stronger. The TPR results showed the existence of a distribution of NiO crystallite sizes having different interactions with the support and these NiO-support interactions in the Ni/ZrO_2–CeO_2 catalysts are quite different than those found in the Ni/single oxide catalysts [30].

The reducibility of the catalysts was also studied by XPS and the results are presented in Table 4. It can be observed that only 50–60% of the Ni^{+2} species present on the surface are reduced after reduction treatment

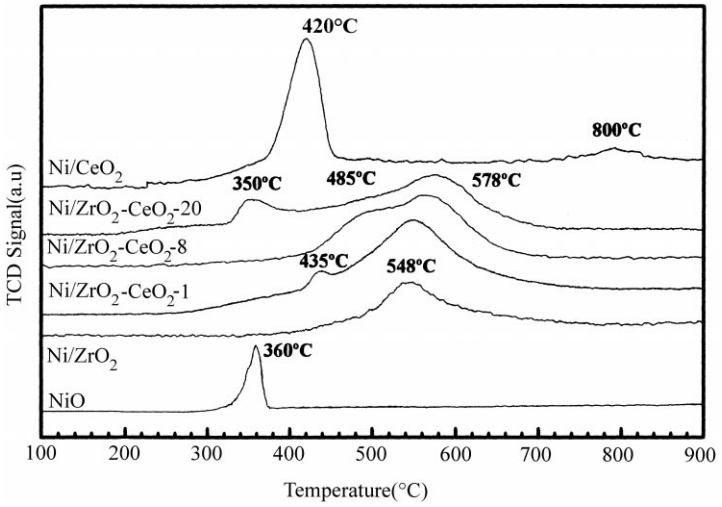

Fig. 4. TPR profiles of the catalysts calcined at 800°C.

Table 4
Surface reducibility (%), surface metal ratios (*S*), and bulk metal ratios (*B*) of the catalysts calcined at 800°C and reduced at 500°C obtained by XPS

Cation	Ni/ZrO_2		Ni/ZrO_2–CeO_2-1		Ni/ZrO_2–CeO_2-8		Ni/ZrO_2–CeO_2-20	
	Calcined	Reduced	Calcined	Reduced	Calcined	Reduced	Calcined	Reduced
Ni^{2+}	100	55	100	30	100	50	100	40
Ni^0	0	45	0	70	0	50	0	60
Ce^{4+}	–	–	–	–	70	70	78	70
Ce^{3+}	–	–	–	–	30	30	22	30
Ni/Zr-*S*	0.12	0.05	0.14	0.15	0.21	0.13	0.23	0.2
Ni/Zr-*B*	0.23	–	0.302	–	0.294	–	0.33	–
Ce/Zr-*S*	–	–	–	–	0.08	0.07	0.17	0.16
Ce/Zr-*B*	–	–	0.004	–	0.071	–	0.244	–

at 500°C. In general the degree of reduction increases with the ceria content. In addition, the presence of Ce^{+3} is detected in the samples with higher CeO_2 content. This partial reduction of Ce^{4+} can be achieved during the XPS pretreatment under vacuum [32,33] and attributed to the progressive elimination of surface hydroxyl groups and oxygen in the CeO_2 surface. This agrees with the XRD results, indicating the presence of segregated ceria in the Ni/ZrO_2–CeO_2-20 sample. For the Ni/ZrO_2–CeO_2-8 sample the Ce^{4+}/Ce^{3+} ratio was not modified by the reduction process, suggesting that Ce^{4+} and Ce^{3+} are either incorporated into the t-ZrO_2 or segregated but with smaller crystal size than detected by XRD.

Table 4 also shows a comparison between the surface composition determined by XPS (represented by the Ni/Zr ratio) and the bulk composition, measured by plasma emission. It is observed that, at low ceria contents, the Ni/Zr surface ratio was smaller than the Ni/Zr bulk ratio. This fact indicates that the surface NiO is agglomerated and forms particles on the ZrO_2–CeO_2 surface, which were detected by XRD. However, when the ceria content is higher, the difference between the bulk and surface ratios is lower, indicating higher homogeneity and better dispersion of the NiO particles on the catalyst surface. Results from XRD showed that in all the samples the Ni^0 particles after reaction presented a similar average size than NiO particles before reduction. This means that active metal sintering is not an important process during the reduction and reforming reaction. Thus the loss in the Ni/Zr ratio for the Ni/ZrO_2 catalyst caused by the reduction process may suggest that Ni particles are partially occluded by the support (by phase sintering and transformation). Moreover, under the same treatment conditions, covering of active metal particles by partially reduced zirconia support (due to strong metal–support interactions) has been previously reported [34].

Also from Table 4 it can be observed surface ceria segregation for the Ni/ZrO_2–CeO_2-20 catalyst, because its Ce/Zr surface ratio is lower than the bulk ratio, while for the Ni/ZrO_2–CeO_2-8 sample both ratios are quite similar.

3.6. Catalytic activity

Fig. 6 presents the evolution over time of CH_4 and CO_2 conversions at a reaction temperature of 800°C and a feed molar ratio $CH_4/CO_2 = 1$. In order to make appropriate comparisons with other experimental results presented in the literature, it must be taken into account that the space velocity used in this work (WHSV: 190 800 lt/kg/h) is one of the highest to be found in the literature. Bradford and Vannice [7] have shown, from kinetics data in the literature that the use of low space velocity may frequently modify the catalytic activity and the apparent activation energy due to the proximity of thermodynamic equilibrium.

It can be observed from the results in Fig. 5 that catalysts containing Ni supported on pure oxides (ZrO_2 and CeO_2) presented similar conversions (below 15%), and that these were the lowest obtained. When ceria is added to the Ni/ZrO_2 catalyst a significant increase in conversion is noticed. As a general trend, CH_4 and CO_2 conversions increased according to the CeO_2 content. Thus the activity of the samples is related to their reducibility, i.e. to the quantity of Ni^0 present on the surface (see Fig. 4 and Table 4).

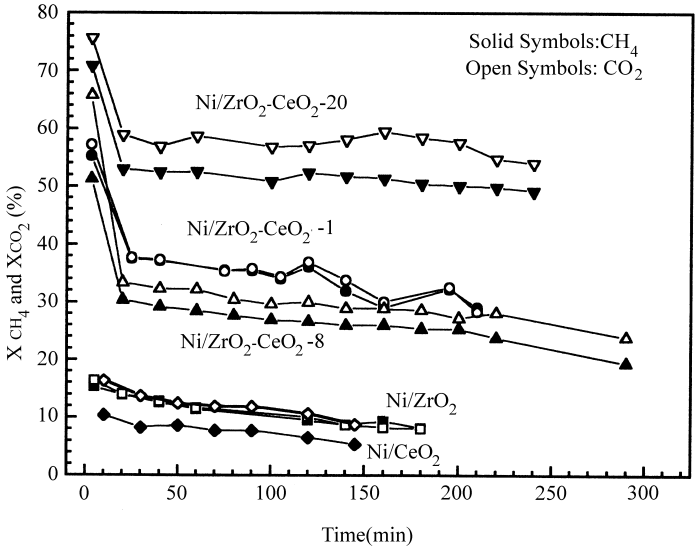

Fig. 5. Catalytic activity of catalysts during reforming of CH_4 with CO_2 at 800°C and $CH_4/CO_2 = 1$ feed ratio.

The activity of the Ni/ZrO_2–CeO_2-8 catalyst is lower activity than that of the Ni/ZrO_2–CeO_2-1. This is related to its particular properties as indicated by the TPR and XPS results of this sample (lower reducibility and lower Ni/Zr ratio than the other ceria containing catalysts).

CO_2 conversion has always been found to be higher than CH_4 conversion (Fig. 5) because the reverse water-gas shift (RWGS) reaction occurs simultaneously with CO_2 reforming of CH_4 [7]. For this reason, the H_2/CO ratio always attains values lower than unity (Fig. 6). Although at the high temperature used in the experiments, the thermodynamic equilibrium of all the species leads to a diminution of water formation [7], this product was detected in all cases, as a consequence of the existence of the RWGS re-

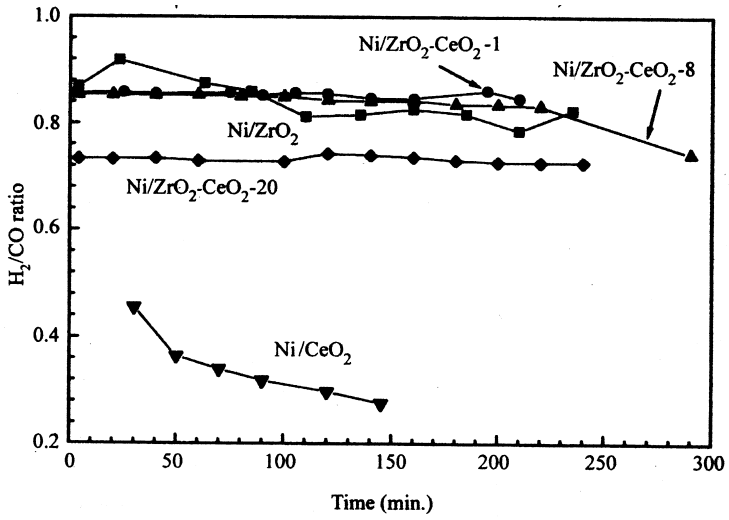

Fig. 6. H_2/CO ratio obtained during reforming of CH_4 with CO_2 at 800°C and $CH_4/CO_2 = 1$ feed ratio.

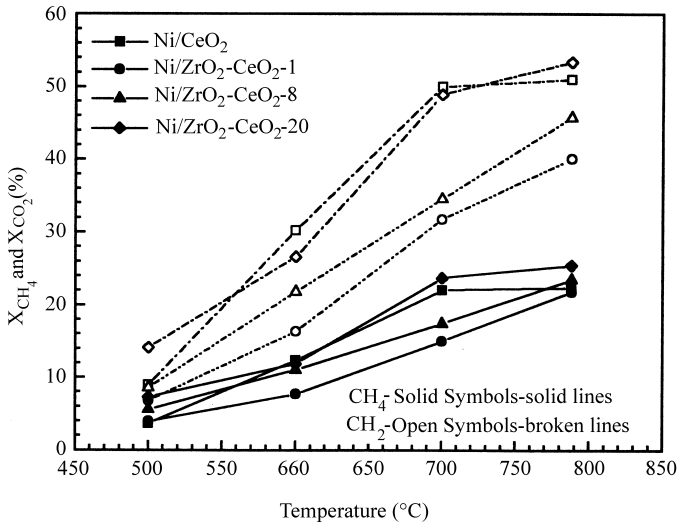

Fig. 7. Evolution of catalytic activity with reaction temperature for reforming of CH_4 with CO_2 using $CH_4/CO_2 = 2$ feed ratio.

action. However, some differences can be observed. Thus, for Ni/ZrO_2 and Ni/ZrO_2–CeO_2-1 catalysts, the conversions attained are very close, suggesting a similarity in the nature of the catalysts and that a 1 wt.% of CeO_2 does not much modify the catalytic behavior of Ni/ZrO_2 for the RWGS reaction. When the CeO_2 concentration was increased, the CO_2 conversion became higher than the conversion of CH_4, and this can only be due to a enhancement of the RWGS reaction. Consequently the H_2/CO ratio is decreased (Fig. 6). Ni/CeO_2 exhibited the lowest H_2/CO ratio, indicating the highest extension of the RWGS reaction for this catalyst.

All the catalysts showed a similar slow deactivation along the reaction time. The deactivation of Ni catalysts during the CO_2 reforming of methane is mainly due to the formation of carbonaceous deposits [16,17,23] and to active metal sintering [35]. Carbon formation is limited by thermodynamics under the experimental conditions used [25], so we expected little activity loss due to carbon deposition. In this case, support sintering (mainly) and phase transformation (Ni/ZrO_2) appear to be the causes of the deactivation process. This is revealed by the t-ZrO_2 crystallite growth and the tetragonal-to-monoclinic transition produced during the reaction (see Fig. 3 and Tables 2 and 3). Although the ceria presence induces a t-ZrO_2 stabilization and an increase in the activity, it does not appear to have any significant influence over the deactivation process. In fact, Fig. 3 shows t-ZrO_2 crystallite growth on all the samples, although with high ceria contents the crystallite sizes attained are lower.

Fig. 7 shows the conversion vs. temperature results using a $CH_4/CO_2 = 2$ feed ratio. The conversion values were taken after 20 min of reaction at each temperature, starting at 500°C. The results presented in this figure showed that an increase in the ceria content produced an increase in the apparent activation energy for both reactants, methane and carbon dioxide, but that the augmentation of the temperature induces a higher activation of the CO_2 than of the CH_4. These facts are related to the mechanism of the reaction [7], which involves the CO_2 adsorption/decomposition over the support or the metal–support interface [36]. This adsorption appears favored over the CeO_2, and as a consequence of the above, the RWGS reaction is enhanced, and the CO_2 conversion increases to a greater degree than the CH_4 conversion.

Fig. 8 shows the results of CH_4 and CO_2 conversions vs. time, at a temperature of 800°C and a ratio of $CH_4/CO_2 = 2$. A trend similar to that in the $CH_4/CO_2 = 1$ experiments was observed. In spite of the fact that these operating conditions can favor carbon formation, a lower deactivation of the catalysts is

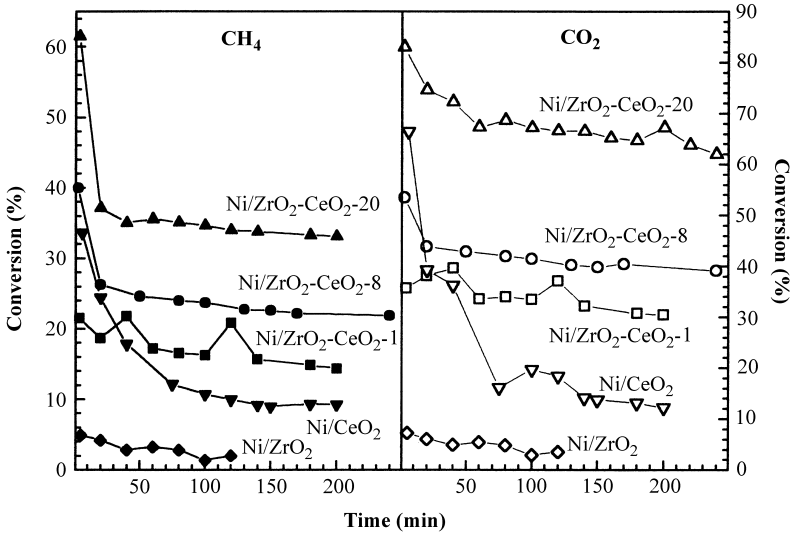

Fig. 8. Catalytic activity of catalysts during reforming of CH_4 with CO_2 at 800°C and $CH_4/CO_2 = 2$ feed ratio: (a) CH_4 conversion and (b) CO_2 conversion.

observed, excepting the Ni/CeO_2 sample, indicating that carbon is not the main cause of the activity loss. The Ni/CeO_2 catalyst showed high initial CH_4 and CO_2 conversions, being under these operating conditions one of the most active catalysts, in contrast to the results obtained at the $CH_4/CO_2 = 1$ ratio. This result suggests that this catalyst needs higher reducing conditions to favor the initial activity. It does, however, suffer fast and drastic deactivation over time. This deactivation could be caused by the existence of a "strong metal–support interaction", when the catalysts are reduced at high temperature [37,38]. Thus,

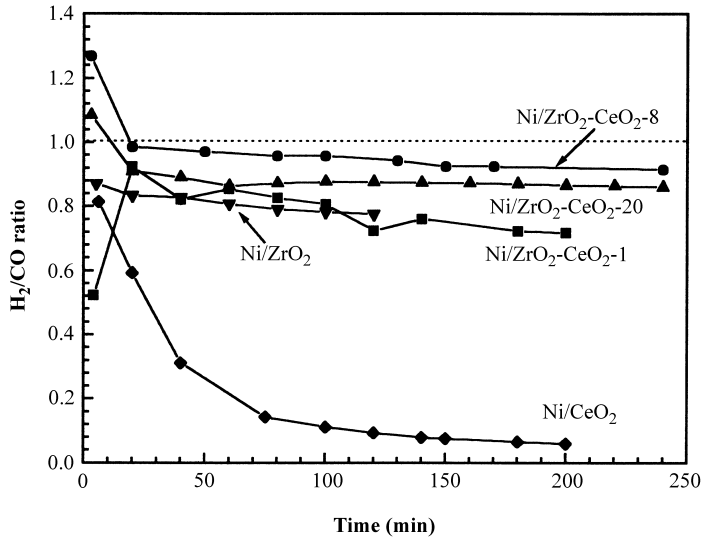

Fig. 9. H_2/CO ratio obtained during reforming of CH_4 with CO_2 at 800°C and $CH_4/CO_2 = 2$ feed ratio.

Daniel [38], using IR spectroscopy, found that the CO chemisorption capability was strongly diminished only when the reduction temperature was increased from 400 to 700°C, pointing out that the temperature onset for SMSI effects on M/CeO_2 could be higher than on M/TiO_2 (M: transition metal). The existence of this temperature onset for SMSI effect was confirmed by TEM [39,40]. This effect could be occurring in our case, given that the reaction temperature (800°C) is higher than that onset, and the reaction atmosphere is reducing.

As can be observed in Fig. 9, the values of the H_2/CO ratio for the $CH_4/CO_2 = 2$ experiments exhibited a similar behavior than those obtained for $CH_4/CO_2 = 1$, with the exception of Ni/CeO_2. The ceria containing catalysts attained H_2/CO ratios close to unity. However, Ni/CeO_2 initially presented a high H_2/CO ratio but this quickly decreased over time. It is observed that the H_2 production drastically diminished whereas the CO formation presented a slower drop. This fact could be caused by partial reduction of the support, as it is shown in Fig. 4 (reduction peak at 800°C) and mainly by the existence of the RWGS reaction. It seems that both processes, loss of activity and enhancement of the RWGS reaction, are consequences of the changes in the catalyst due to the existence of strong metal–support interactions.

3.7. Carbon formation

Results of experiments in the thermobalance, at 700°C and with a $CH_4/CO_2 = 1$ ratio, are shown in Fig. 10. The rate and total amount of carbon formation over the catalysts followed the same pattern as the catalytic activity (see Fig. 5), obtaining that an increase in the ceria content enhances the carbon formation. The lowest carbon deposition was exhibited by the Ni/ZrO_2 and Ni/CeO_2 catalysts due to their low catalytic activity.

The TEM observations showed the presence of carbon filaments over the samples after reaction at 800°C (Fig. 11). The carbon structure was graphitic with the usual constant spacing between layers. Graphitic filaments were reported previously in Ni catalysts after the dry reforming reaction, also at the same temperature of 700°C [3,35]. The metal particles at the end of the filaments have the characteristic pear form, in accordance with the mechanism proposed by Snoeck et al. [41]. Furthermore, there are filaments of different diameters indicating the presence of a distribution of Ni crystallite sizes. It is worth mentioning that for every catalyst the filament zones were not present on the whole surface; it was necessary to localize them. The carbon amounts are therefore really small. This observation is consistent with the non-presence of graphite XRD reflection in the catalysts after reaction, and with

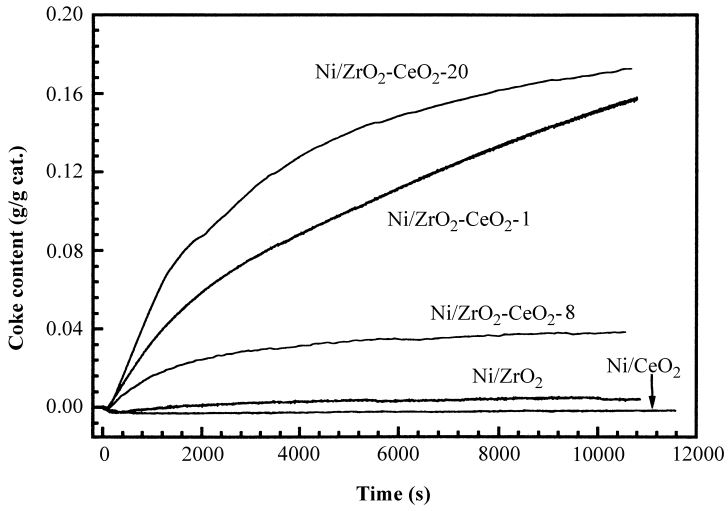

Fig. 10. Thermobalance experiments of carbon formation during reforming of CH_4 with CO_2 at 700°C and $CH_4/CO_2 = 1$ feed ratio.

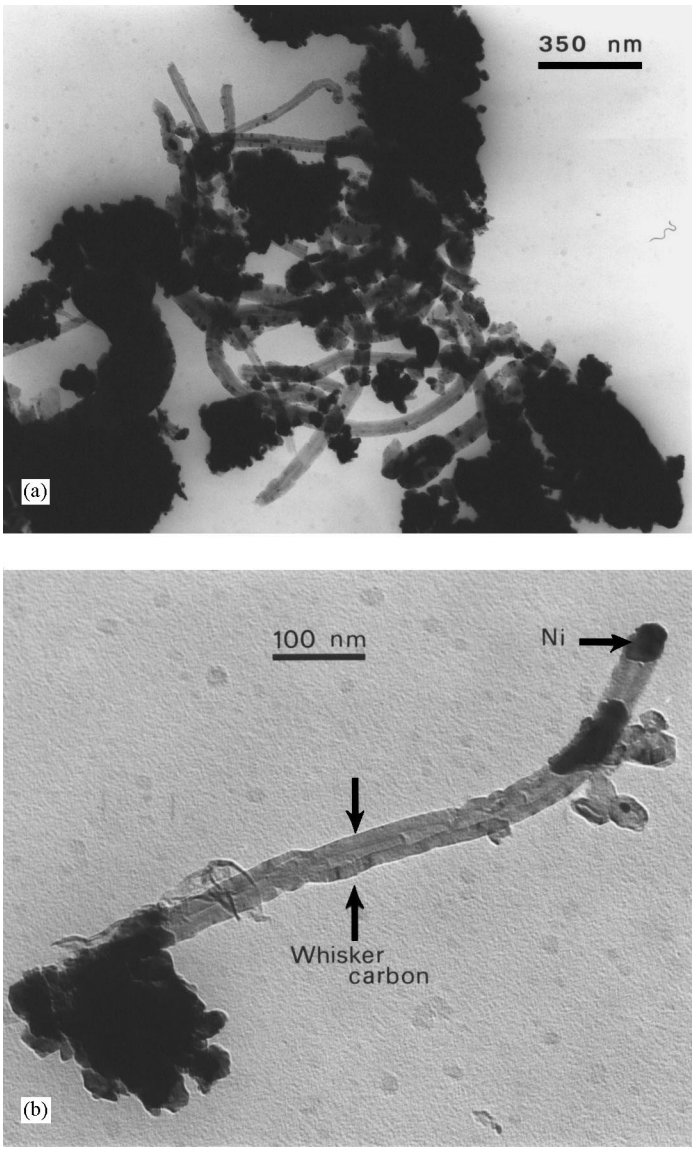

Fig. 11. TEM images of graphitic filaments formed on the catalysts during reforming of CH_4 with CO_2 at 800°C and $CH_4/CO_2 = 1$ feed ratio: (a) Ni/ZrO_2–CeO_2-1 sample and (b) Ni/ZrO_2–CeO_2-20 sample.

the thermodynamic considerations [25]. Formation of carbon deposits may occur through both methane decomposition and CO disproportionation (Boudouard reaction):

$$CH_4 \rightleftarrows C + H_2 \quad (\Delta H^0 = 17.9\,\text{kcal/mol C}),$$
$$2CO \rightleftarrows CO_2 + C \quad (\Delta H^0 = -41.2\,\text{kcal/mol C})$$

At higher reaction temperatures, carbon is mainly produced from CH_4, but when the temperature decreases CO disproportionation becomes predominant. The results of Reitmeier et al. [42] and Richardson and Paripatyadar [43] indicate that CO is the main contributor to the formation of graphitic carbon, which agrees with the results obtained by Swaan et al. [11]

and Tsipouriari et al. [44] using isotope labeling and TPO techniques.

The concentrations of carbon obtained in the thermogravimetric system at 700°C are higher than those obtained in the fixed-bed plant at 800°C. In fact, the graphite presence was detected by XRD (peak at $2\theta = 26.4$) in the catalysts after reaction in the thermobalance (results not shown).

This difference can be explained taking into account the endothermic character of the reaction and the position of the thermocouple in the thermobalance, outside of the sample. Thus activity measurements in the thermobalance can be masked by a difference of temperature between the sample and the thermocouple, the real temperature in the sample being lower than the nominal set point temperature indicated by the thermocouple. In the fixed-bed reactor, the decrease of the temperature in the sample at the beginning of the reaction is detected by the thermocouple and then corrected by the control loop. Therefore the more reactive the catalyst is, the higher the temperature falls at the beginning of the reaction and the more coke is produced.

4. Conclusions

The sol–gel catalyst preparation method allows the homogeneous incorporation of high amounts of Ni and Ce to the t-ZrO_2 lattice. A solid solution was then achieved incorporating CeO_2 (up to 20 wt.%) to ZrO_2, and partial incorporation of Ni^{2+} to the lattice was also detected. The zirconia tetragonal phase (t-ZrO_2) stability was enhanced by CeO_2 addition, while the mean crystallite size was diminished. The higher the quantity of ceria present, the smaller the t-ZrO_2 crystallite and the greater the inhibition of tetragonal-to-monoclinic phase transformation. However, support sintering after the reforming reaction at 800°C is not totally avoided after ceria addition. In addition, it is obtained that the BET surface area of the Ni/ZrO_2–CeO_2 catalysts are slightly higher than Ni over single oxides samples.

TPR and XPS results showed that the increase of both the reducibility of NiO and the Ni^0 surface dispersion increase as the CeO_2 content becomes higher. These facts strongly affect the catalytic activity, obtaining that an increase in the ceria content in the support enhances the conversion attained. The Ni/CeO_2 sample exhibited a particular behavior, probably due to the presence of "strong metal–support interaction" phenomenon. CeO_2 also induces a larger difference between CO_2 and CH_4 conversions and a lowering of the H_2/CO ratio, thus enhancing the RWGS reaction during dry reforming of methane.

Carbon formation did not appear to be the main cause of the activity loss. The catalyst deactivation is a consequence of the phase transition and support sintering produced at the beginning of the reaction. TEM observations showed that the carbon was deposited over the catalysts in the form of graphitic filaments of different diameters depending on the Ni crystal size.

Acknowledgements

The authors acknowledge financial support from DGES-MEC (Madrid) (Project PB97-1020). J.A.M. acknowledges financial support from CONACYT and I.M.P. (Mexico).

References

[1] S. Wang, G.Q. (Max) Lu, Energy & Fuels 10 (1996) 896.
[2] J.R. Rostrup-Nielsen, J.-H. Bak Hansen, J. Catal. 144 (1993) 38.
[3] S. Wang, G.Q. Lu, Appl. Catal. 169 (1998) 271–280.
[4] S. Wang, G.Q. Lu, Appl. Catal. B 16 (1998) 269–277.
[5] T. Osaki, T. Horiuchi, et al., Catal. Lett. 52 (1998) 171–180.
[6] M.E.S. Hegarty, A.M. O'Connor, J.R.H. Ross, Catal. Today 42 (1998) 225.
[7] M.C.J. Bradford, M.A. Vannice, Catal. Rev.-Sci. Eng. 41 (1) (1999) 1–42.
[8] J.A. Lercher, J.H. Bitter, W. Hally, W. Niessen, K. Seshan, Stud. Surf. Sci. Catal. 101 (1996) 463.
[9] K. Tomishige, Y.-G. Chen, K. Fujimoto, J. Catal. 181 (1999) 91.
[10] V.A. Tsipouriari, X.E. Verykios, J. Catal. 187 (1999) 85.
[11] H.M. Swaan, V.C.H. Kroll, G.A. Martin, C. Mirodatos, Catal. Today 21 (1994) 571.
[12] M.C.J. Bradford, M.A. Vannice, Appl. Catal. A 142 (1997) 73.
[13] M.C.J. Bradford, M.A. Vannice, Appl. Catal. A 142 (1997) 97.
[14] Y. Chen, K. Tomishige, K. Yokoyama, K. Fujimoto, J. Catal. 184 (1999) 479.
[15] M.C.J. Bradford, M.A. Vannice, Catal. Today 50 (1999) 47.
[16] S. Wang, G.Q. (Max) Lu, Ind. Eng. Chem. Res. 38 (1999) 2615.
[17] Y.-H. Chen, J. Ren, Catal. Lett. 29 (1994) 39.

[18] T. Yamaguchi, Catal. Today 20 (1994) 199.
[19] G. Centini, G. Cerrrato, S.D. Angelo, U. Finardi, E. Giamello, C. Morterra, S. Perathoner, Catal. Today 27 (1996) 265.
[20] R.C. Garvie, J. Phys. Chem. 69 (1965) 1238.
[21] R.C. Garvie, J. Phys. Chem. 82 (1978) 218.
[22] M. Yashima, N. Ishizawa, M. Yoshimura, J. Am. Ceram. Soc. 75 (6) (1992) 1550.
[23] Z.L. Zhang, X.E. Verykios, Catal. Today 21 (1994) 589.
[24] Z. Cheng, Q. Wu, J. Li, Q. Zhu, Catal. Today 30 (1996) 147.
[25] A.M. Gadalla, B. Bower, Chem. Eng. Sci. 43 (11) (1988) 3049.
[26] E. Gamas, Ph.D. Thesis, Texas University, Texas, May 1996.
[27] S. Rossignol, Y. Madier, D. Duprez, Catal. Today 50 (1999) 261.
[28] C.E. Hori, H. Permana, K.Y. Simon, A. Brenner, K. More, K.M. Rahomoeller, D. Belton, Appl. Catal. B 16 (1998) 105.
[29] A. Trovarelli, Catal. Rev.-Sci. Eng. 38 (1996) 439.
[30] P. Fornasiero, R. Di Monte, G. Ranga Rao, J. Kaspar, S. Meriani, A. Trovarelli, M. Graziani, J. Catal. 151 (1995) 168.
[31] S. Tang, J. Lin, K.L. Tan, Catal. Lett. 51 (1998) 169.
[32] J.L.G. Fierro, J. Soria, J. Sanz, J.M. Rojo, J. Solid State Chem. 66 (1987) 154.
[33] S. Bernal, J.J. Calvino, G.A. Cifredo, J.M. Rodríguez-Izquierdo, V. Perrichon, A.A. Laachir, J. Catal. 137 (1992) 1.
[34] S.M. Stagg-Williams, R. Soares, E. Romero, A. Pisanu, W.E. Alvarez, D.E. Resasco, Stud. Surf. Sci. Catal 130 (2000) 3663.
[35] V.C.H. Kroll, H.M. Swaan, C. Mirodatos, J. Catal. 161 (1996) 409.
[36] J.H. Bitter, K. Seshan, J.A. Lercher, J. Catal. 176 (1998) 93.
[37] P. Meriaudeau, J.F. Dutel, M. Dufaux, C. Naccache, Stud. Surf. Sci. Catal. 11 (1982) 95.
[38] D.W. Daniel, J. Phys. Chem. 92 (1988) 3891.
[39] S. Bernal, J.J. Calvino, J.M. Gatica, C. Larese, C. López-Cartes, J.A. Pérez-Ormil, J. Catal. 169 (1997) 510.
[40] S. Bernal, J.J. Calvino, M.A. Cauqui, J.M. Gatica, C. Larese, J.A. Perez Ormil, J.M. Pintado, Catal. Today 50 (1999) 175.
[41] J.W. Snoeck, G.F. Froment, M. Fowlest, J. Catal. 169 (1997) 240.
[42] R.E. Reitmeier, K. Atwood, H.A. Bennet Jr., H.M. Baugh, Ind. Eng. Chem. 40 (1948) 620.
[43] J.T. Richardson, S.A. Paripatyadar, Appl. Catal. 61 (1990) 293.
[44] V.A. Tsipouriari, A.M. Efstathiou, Z.L. Zhang, X.E. Verykios, Catal. Today 21 (1994) 579.